Galvanostatically Deposited PtNi Thin-Films as Electrocatalysts for the Hydrogen Evolution Reaction

Alejandra Medrano-Banda, Alfonso Crespo-Yapur, Miguel Ángel Velasco-Soto, and Marcelo Videa*[a]

The synthesis of hybrid platinum materials is fundamental to enable alkaline water electrolysis for cost-effective H_2 generation. In this work, we have used a galvanostatic method to co-deposit PtNi films onto polycrystalline gold. The surface concentrations of Ni (Γ_{Ni}) and Pt (Γ_{Pt}) were calculated from electrochemical measurements; the Γ_{Pt}/Γ_{Ni} ratio and electrocatalytic activity of these materials towards hydrogen evolution reaction (HER) in 1 M KOH show a strong dependence on the current density pulse applied during the electrodeposition. Analysis of the Tafel parameters hints that, on these deposits, HER proceeds through a Volmer-Heyrovsky mechanism. The galvanostatically deposited PtNi layers present a high current output per Pt gram, 3199 $A g_{Pt}^{-1}$, which is significantly larger compared to other PtNi-based materials obtained by more extended and more complex synthesis methods.

Introduction

The need to phase out fossil fuels to minimize global warming has led to the search for alternative energy carriers and energy storage systems. Among them, molecular hydrogen stands out since it has a high energy density (4 kWh/kg), and its use produces no carbon emissions.[1,2] Currently, hydrogen is produced mainly by steam reforming, which consumes fossil fuels and prevents hydrogen-based technologies from being carbon neutral. Although water splitting is a cleaner method for H_2 synthesis, economic limitations have prevented it from playing a more significant role in H_2 production.[3,4]

Water splitting comprises two half-reactions: the oxygen evolution reaction (OER) at the anode and the hydrogen evolution reaction (HER) at the cathode. The leading electrolyzers for low-temperature water splitting are proton exchange membrane (PEM) and alkaline; in both cases, Pt, a scarce and expensive metal, has the highest electrocatalytic activity for HER, among the pure metals. HER kinetics is significantly faster in acidic media than in alkaline media, making PEM electrolyzers efficient but expensive devices. However, alkaline electrolyzers present higher durability and, because alkaline media enables the use of non-noble metals as catalysts, lower prizes.[3–5] In alkaline media, HER involves two stages: first, the dissociation of water or Volmer step [Eq. (1)]:

$$H_2O + e^- \leftrightarrows H_{ad} + OH^- \quad \text{Volmer} \tag{1}$$

followed by the recombination of adsorbed hydrogen atoms, H_{ad}, which occurs via the Heyrovsky or the Tafel step [Eq. (2 and 3)]:

$$H_2O + H_{ad} + e^- \leftrightarrows H_2 + OH^- \quad \text{Heyrovsky} \tag{2}$$

$$2H_{ad} \leftrightarrows H_2 \quad \text{Tafel} \tag{3}$$

Noble metals like Pt owe their high catalytic activity for HER to their affinity for hydrogen adsorption and to facilitate H_{ad} recombination. However, they tend to be poor materials for cleaving the H-OH bond required for the Volmer step. On the other hand, non-noble oxophilic transition metals, while poor catalysts for the recombination step, are quite efficient for water dissociation.[6,7] Under this rationale, the design of electrocatalytic materials focuses on combining Pt with transition metals with the additional benefit of cost reduction by decreasing the amount of Pt. Pt-based materials such as Pt/Cu nanoparticles,[8] Pt–Co alloys,[9] and Pt–Ni nanowires[10] have shown high catalytic activity for HER. Pt–Ni materials have attracted attention as electrocatalysts for alcohol oxidation,[11–13] oxygen evolution reaction (OER),[14,15] oxygen reduction reaction (ORR),[15–17] and peroxide sensors.[18,19]

Materials that combine Pt and Ni in different compositions have exhibited an excellent catalytic activity for HER, such as Pt–Ni nanowires,[10] $Ni(OH)_2$-modified Pt electrodes,[20] PtNi nanoparticles,[14,21,22] PtNi nanodendrites,[23] and PtNi–O nanostructures.[24] Most of these materials are generally synthesized by solvothermal methods that involve many steps and can take several hours.[14,15,23] In contrast, electrochemical deposition is a fast and straightforward method that allows high control over the deposits' morphology. Our group

[a] A. Medrano-Banda, Dr. A. Crespo-Yapur, Dr. M. Á. Velasco-Soto, Dr. M. Videa
School of Engineering and Sciences
Tecnologico de Monterrey
Av. E. Garza Sada 2501 Sur
Monterrey, N.L. c.p. 64849 (México)
E-mail: mvidea@tec.mx

Supporting information for this article is available on the WWW under https://doi.org/10.1002/open.202100241

previously used single-pulse galvanostatic electrodeposition to generate Ni thin-layers on a Au electrode; the Ni deposits exhibit high catalytic activity for methanol electro-oxidation.[25] The same methodology can be used to obtain NiMo deposits with HER activity in acidic media.[26] Herein we report a systematic study on the influence of the applied current density on the PtNi deposit's activity and surface composition for HER in alkaline media.

Results and Discussion

PNi Electrodeposition

Subjecting the working electrode to constant current results in a fast polarization until a potential value at which the charge transfer demand can be satisfied by a redox reaction is reached. For an outer-sphere electrochemical reaction, once this happens, the polarization slows down until diffusion of the electroactive species becomes insufficient to maintain the current, which prompts a polarization towards a more negative potential. Sand's equation gives an estimate of the characteristic time of a diffusion-controlled process [Eq. (4)]:

$$\tau^{1/2} = \frac{nF(D\pi)^{1/2}c^*}{2j} \quad (4)$$

where n is the number of transferred electrons, F is the Faraday constant, j is the applied current density, D is the diffusion coefficient, and c^* the bulk concentration of the electroactive species, respectively.[28]

This behavior is not observed when reducing the electroactive species results in a new phase, like in electrodeposition. First, the electrode polarizes, passing through a minimum potential value; during this stage, the nuclei of the electrodeposited phase are formed. Then, the potential recovers to stabilize at a value at which the nuclei grow at a rate determined by the galvanostatic current density.[29,30] Under diffusion-limited conditions, the duration of the growth stage follows equation 4.[31,32]

Figure 1a shows the E versus t transient response to a cathodic current pulse of 8 mA cm^{-2} gold electrode immersed in the plating bath (50 mM $NiCl_2$ + 1.5 mM $K_2[PtCl_4]$ + 500 mM NaCl, the pH 2.0). The stepped characteristics of the potential transient hint at least four electrochemical processes occurring in different time domains, identified as regions I to IV [Eq. (5–8)]. The discontinuous horizontal lines in Figure 1a indicate the Nernst potentials of reactions that may take place on the working electrode.

$$PtCl_4^{2-} + 2e^- \leftrightarrows Pt^0 + 4Cl^- \quad E = 0.675\,V \text{ vs. RHE} \quad (5)$$

$$2H^+ + 2e^- \leftrightarrows H_2 \quad E = -0.118\,V \text{ vs. RHE} \quad (6)$$

$$Ni^{2+} + 2e^- \leftrightarrows Ni^0 \quad E = -0.289\,V \text{ vs. RHE} \quad (7)$$

$$2H_2O + 2e^- \leftrightarrows H_2 + 2OH^- \quad E = -0.710\,V \text{ vs. RHE} \quad (8)$$

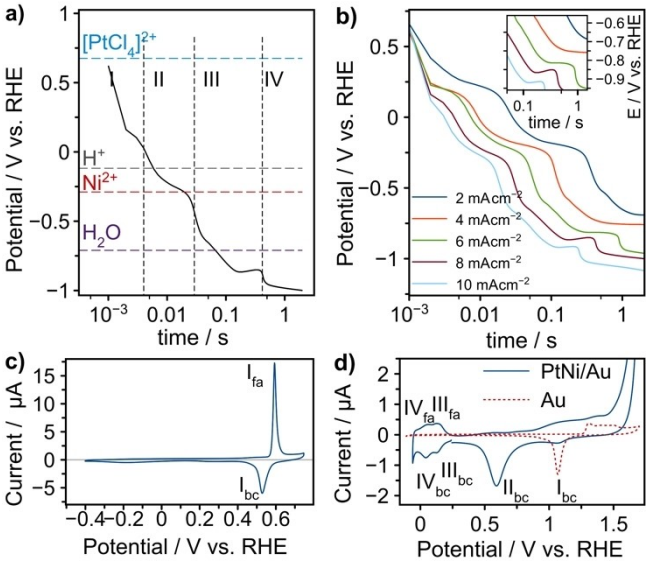

Figure 1. a) Typical potential transient recorded during the galvanostatic deposition of PtNi on a clean Au electrode from a 1.5 mM $K_2[PtCl_4]$ + 50 mM $NiSO_4$ + 500 mM NaCl pH = 2.0 plating bath. j_{dep} = 8.0 mA cm^{-2}. b) Potential transients recorded during a galvanostatic deposition of PtNi on a clean Au electrode at j_{dep} of 2 to 10 mA cm^{-2}. Inset: close-up to the potential minima of region III. [Notice that the time scale in a) and b) is logarithmic.] c) Cyclic voltammogram of electrodeposited PtNi films at 0.05 V s^{-1} in 1 M KOH indicating the presence of Ni. d) Cyclic voltammogram of electrodeposited PtNi films at 0.05 V s^{-1} in 50 mM H_2SO_4 showing the typical characteristics of hydrogen adsorption and desorption on Pt and reduction peak of platinum monolayer oxide.

Increasing j_{dep} shifts the electrode's potential towards more negative values and shortens the duration of the time domains, as can be seen in Figure 1b. Region IV can only be observed at current density values higher than 4 mA cm^{-2}.

Lin-Cai et al.[33] studied Pt electrodeposition from $[PtCl_4]^{2-}$ by cyclic voltammetry on gold and glassy carbon from a 10 mM $K_2[PtCl_4]$ + 0.5 M H_2SO_4. They observed a wave positive to the Pt(II)/Pt peak around −0.40 V versus RHE; this feature was not observed for Pt electrodeposition on glassy carbon. The authors suggest that this wave corresponds to an initial Pt monolayer's formation before the onset of bulk Pt electrodeposition. Liu et al.[34] observed a similar pre-wave between −0.49 V and −0.24 V versus RHE during the electrodeposition of Pt on gold by linear sweep voltammetry.

Electrochemical quartz crystal microbalance (EQCM) measurements performed during the electrodeposition showed that this wave is concomitant to a mass increment, suggesting that it is caused by Pt deposition. This pre-wave is located within Region I's potential window while Region II coincides with the location main Pt deposition peaks observed during cyclic voltammetry. No nucleation minima were observed in regions I and II; however, the potentials reached in region II favor Pt electrodeposition. The galvanostatic deposition of Pt was carried out on glassy carbon and on a 50 nm thick vapor deposited Au sputtered on a Si wafer. Using a plating solution of 1.5 mM $K_2[PtCl_4]$ and pH = 2.0, and a j_{dep} of 4.0 mA cm^{-2}, the resulting curves show that deposition on glassy carbon requires larger polarization compared to Au (see Figure S1). Further-

more, while both potential transients exhibit the expected deposition minima, in the Au/Si electrode is less evident. The difference between the minimum potential reached during the nucleation stage and the stabilization potential for this electrode is 124 mV, while for the glassy carbon electrode is 200 mV. The galvanostatic deposition proceeds at low overpotentials suggesting the high affinity of Pt for Au, which leads to barely noticeable deposition minimum, as observed for PtNi electrodeposition.

Region III starts well below the Nernst potential for Ni^{2+} reduction, which suggests that this is the active process in this region. As can be observed in Figure 1b inset, the shape of the potential transient in region II changes as the j_{dep} is increased, revealing the characteristic nucleation minimum.[29,30] It has been reported that water reduction (reaction 9) occurs simultaneous to Ni^{2+} reduction and may play a role in it;[35–37] thus, it is plausible that it also takes place in region III. Finally, region IV can be assigned mainly to water reduction, which may proceed once proton reduction is finished.

Figure 1c shows the voltammogram of a PtNi deposit generated at 8 mA cm^{-2} in 1 M KOH. Peaks I_{fa} and I_{bc} correspond to the formation and reduction of NiOOH according to Equation (9),[38,39] thus confirming the presence of Ni on the deposit:

$$Ni(OH)_2 + OH^- \leftrightarrows NiOOH + e^- \quad (9)$$

Figure 1d presents the voltammograms obtained in 50 mM H_2SO_4 before (dashed line) and after (solid line) the electrodeposition experiment. Peak I_{bc} corresponds to the reduction of a gold oxide monolayer formed during the anodic scan. After the electrodeposition stage, the gold features are no longer observed and are replaced by those of Pt, that is, an earlier onset of oxide formation and oxygen evolution, a more cathodic reduction peak (II_{bc}), and the characteristic hydrogen adsorption and desorption peaks (III_{bc}, IV_{bc}, III_{fa}, and IV_{fa}). Peak I_{bc} is still visible, although diminished, after the electrodeposition, indicating that a small fraction of the gold's surface is still exposed. For all applied currents, the presence of Ni and Pt was electrochemically confirmed.

SEM inspection of a deposit generated using an 8.0 mA cm^{-2} pulse (Figure 2a) shows no evidence of distinguishable particle formation indicating a layered deposit. Energy-dispersive X-ray (EDX) mapping analysis revealed Ni's presence on the whole electrode surface (Figure 2b and 2c). Pt content on the deposit could not be determined by this method due to the proximity between the Pt and Au signals.

The surface composition of the PtNi deposits can be estimated from the electrochemical data in the voltammograms. The surface concentration of Ni (Γ_{Ni}) can be extracted from the area under the peak I_{af}, Q (Figure 1c) with the following formula (Eq. (10)]:

$$\Gamma_{Ni} = \frac{Q}{nFA_{geo}} \quad [\text{mol cm}] \quad (10)$$

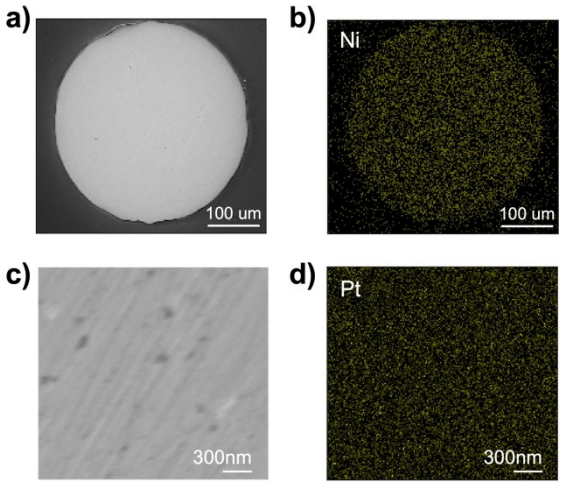

Figure 2. SEM images of PtNi deposited on a Au electrode at 8.0 mA cm^{-2} at two different magnifications a) and c). EDX mapping of b) Ni on the whole electrode and d) Pt.

The available Pt surface area can be computed using Equation (11):

$$ECSA = \frac{Q_{red}}{Q_0} \quad (11)$$

where Q_{red} is the average charge of the adsorption (III_{bc}, IV_{bc}) and desorption (III_{fa}, and IV_{fa}) peaks, and Q_0 is the charge associated with the formation or desorption of a H_{ad} monolayer per square centimeter (210×10^{-6} C cm^{-2}). Considering that the surface atom density for Pt is 1.31×10^{15} cm^{-2},[27] the active Pt surface concentration can be estimated by [Eq. (12)]:

$$\Gamma_{Pt} = \frac{A_{Pt}\rho}{N_A A_{geo}} \quad [\text{mol/cm}] \quad (12)$$

where A_{Pt} is the Pt surface area, ρ is the surface atom density, and N_A is Avogadro's number. Table 1 shows that for all the applied deposition current pulses, the surface concentration of Pt is more than an order of magnitude larger than Ni. Deposition at $j_{dep} = 8.0\times10^{-3}$ A cm^{-2} was performed on an Au/Si electrode. This sample was subjected to an XPS depth profiling test. The results, shown in Figure S2, suggest that the deposit is richer in Pt than in Ni, agreeing with the electrochemical estimations.

Table 1. Surface composition of the PtNi deposits for all cathodic current densities studied was determined from electrochemical measurements.

j_{dep}/ [A cm^{-2}]	$\Gamma_{Ni}/10^{-9}$ [mol cm^{-2}]	$\Gamma_{Pt}/10^{-9}$ [mol cm^{-2}]
2.0×10^{-3}	0.06	4.52
4.0×10^{-3}	0.69	6.15
6.0×10^{-3}	0.41	6.85
8.0×10^{-3}	0.39	7.72
10.0×10^{-3}	0.89	6.25

The experimental τ for Pt averaged from three measurements, and the theoretical values are tabulated in Table 2. These transition times were estimated under the assumption that Pt electrodeposition occurs during regions I and II. There is a good agreement between the theoretical and experimental τ_{Pt} (see Table 2); the latter were calculated using a diffusion coefficient of 2.2×10^{-6} cm^2 s^{-1},[33] and *j* normalized to the Au *ECSA*. This suggests that for Pt deposition, the roughness of the Au electrode plays an important role in defining the diffusion field, even at a time scale of hundreds of milliseconds, and that this process is limited by diffusion.

The experimental τ_{Ni}, shown in Table SI (Supporting Information), were estimated assuming that Ni deposition occurs during region III; values for the 2 and 4 mA cm^{-2} pulses could not be determined since these experiments did not last long enough to observe the end of region III. For the remaining pulses, τ_{Ni} shows a large variation between repetitions. The theoretical transition times were computed assuming a diffusion coefficient of 4×10^{-6} cm^2 s^{-1},[32] and normalizing the applied current to geometric area since the transition times are long enough to disregard roughness effects on the diffusion field.

In all cases, the experimental τ_{Ni} is significantly longer than the theoretical prediction. This behavior could be attributed to hydrogen evolution from the reduction of protons, which takes place in the same potential range of Ni deposition; Figure S3a shows how decreasing the *p*H from 6 to 2 expands the transition time for Ni deposition, most likely because reactions 7 and 8 occur simultaneously. Increasing the *p*H of the PtNi plating solution leads to a significant increase in the NiOOH peak, suggesting that at *p*H 2, hydrogen evolution consumes a significant fraction of the applied charge, decreasing the Nickel deposition efficiency (Figure S3b).

Liu et al.[34] reported that for the electrodeposition of Pt thin-films on gold under potentiostatic control, in which a polarization of −0.159 V versus RHE led to the formation of a 33 nm thick layer after 500 s, while a −0.559 V versus RHE results on the formation of a 0.25 nm thick monolayer, which is terminated after the first second of electrodeposition by the adsorption of H. A similar self-termination process was observed by Wang et al.[40] for Ni electrodeposition on Au by potential pulses negative to the hydrogen evolution onset, the formation of $Ni(OH)_2$ due to a local *p*H rise inhibits further deposition resulting in a thin Ni layer. Applying a potential pulse of −1.259 V versus RHE would result in the formation of a 1 to 2 nm thick Ni layer, depending on the Ni^{2+} concentration of the platting bath. Recently Salinas-Quezada et al.[25] showed that galvanostatic electrodeposition on Ni on Au also leads to the formation of Ni thin-layers.

XPS depth profile analysis of the PtNi deposits formed on the Au/Si samples suggests that the PtNi deposits have a 20 nm thickness. The SEM images of these samples are shown in Figures S4a and S4b. Since the applied charge is the same, and SEM images of both deposits are similar, it can be inferred that a similar thin layer is formed on the Au disk electrodes. Self-termination favors the formation of thin films; however, this cannot be confirmed from the chronopotentiometric data since the reduction of protons does not allow to pinpoint the end of Ni deposition. It is unlikely that Pt self-termination occurred during the PtNi deposition experiments since the experimental transition times are relatively close to the ones predicted by Sand's equation, indicating that the deposition was diffusion limited. However, due to the negative potentials reached during the experiments, the deposited Pt could have been blocked by adsorbed hydrogen, preventing Ni deposition on it, which

Table 2. Comparison between the τ_{Pt} values obtained experimentally, and those predicted by Sand's equation (eqn.4) for all cathodic current densities studied.

J_{dep}/[A cm^{-2}]	Exp. τ_{Pt}/[ms]	Theor. τ_{Pt}/[ms]
2.0×1^{-3}	312 ± 103	362
4.0×10^{-3}	98 ± 12	90
6.0×10^{-3}	46 ± 14	40
8.0×10^{-3}	29 ± 4	23
10.0×10^{-3}	19 ± 1	14

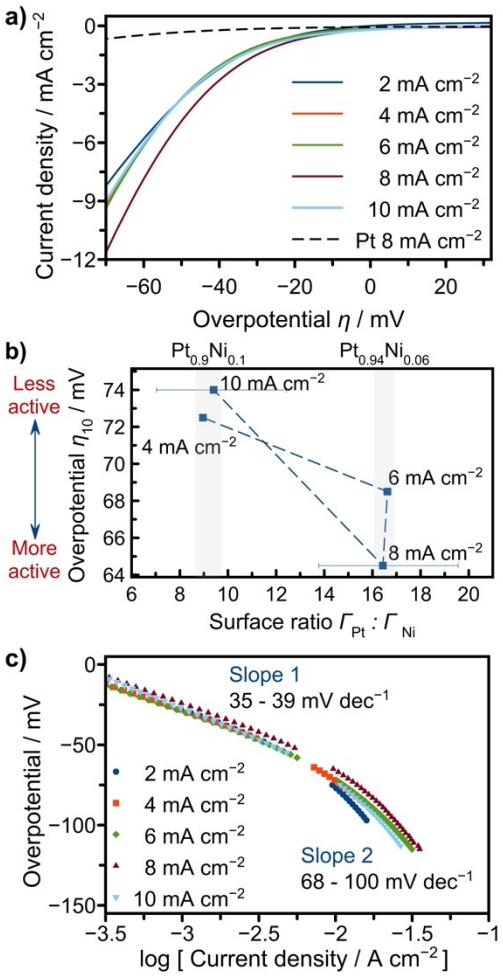

Figure 3. a) Polarization curves in 1 M KOH at 5 mV s^{-1} of gPtNi/Au materials generated at different currents densities. Pt deposited at 8 mA cm^{-2} is included b) dependences of η_{10}, A_{Pt}, and Γ on the applied deposition current densities. PtxNi(1–x) proportions are calculated from the ratios of the areas Γ_{Pt}:Γ_{Ni} c) Tafel slopes of the materials deposited at different current densities.

would account for the high Pt surface concentration; however, contributions of surface segregation cannot be discarded.

The SEM, EDX mapping, and electrochemical characterizations suggest that galvanostatic electrodeposition on gold leads to the formation of thin-films PtNi, with both species present on the deposit's surface.

HER Electrocatalysis

The linear sweep voltammograms (LSV) of the galvanostatically deposited PtNi materials (G-PtNi/Au) generated at different j_{dep} values are shown in Figure 3a. The LSV curves current was normalized to the electrode's geometric area, and their electrocatalytic performance was evaluated by the overpotential they required to reach 10 mA cm^{-2}, η_{10}. The material deposited at 8 mA cm^{-2} exhibits the lowest overpotential, 64 mV, while the highest overpotential value was 77 mV, which corresponds to the 2 mA cm^{-2} deposit. For comparison, the black line corresponds to a Pt deposit generated at 8 mA cm^{-2} in an electrochemical bath containing a similar composition to the PtNi one (1.5 mM $K_2[PtCl_4]$ + 500 mM NaCl *p*H = 2.0). The inferior catalytic activity makes it evident that, despite the high Pt surface concentration of the PtNi deposits, the presence of Ni has an impact on their performance.

Figure 3b shows the dependence of the averaged observed overpotential at 10 mA cm^{-2} (η_{10}), on the ratio the Γ_{Pt}:Γ_{Ni} ratio, the j_{dep} values are written next to the corresponding points.

The value of the current density j_{dep} seems to have an important effect on the Γ_{Pt}:Γ_{Ni} ratio, with pulses of 2, 4, and 10 mA cm^{-2} generation deposits with ratios smaller than 10, while pulses of 6 and 8 mA cm^{-2} generate deposits with ratios higher than 13. The latter pulses are the ones that exhibit the lowest overpotential, which suggests that the Pt Γ_{Pt}:Γ_{Ni} ratio has high importance on the catalytic activity of the deposits, and that values between 6 and 8 mA cm^{-2} yield deposits with a Γ_{Pt}:Γ_{Ni} ratio that significantly enhances the activity of the materials for HER.

For all the LSV data, the Tafel plots exhibit two regions (see Figure 3c), one from 0 to −50 mV and another one from −90 to −116 mV. The Tafel slopes of both regions are presented in Table 3; values are around 35 mV dec^{-1} for the first slope and 100 mV dec^{-1} for the second and are almost independent of j_{dep}, suggesting that the hydrogen evolution process follows the same pathway on all the PtNi deposits produced. This behavior is similar to the one reported by Shinagawa et al.,[41] for simulations in which Heyrovsky's reaction was the limiting step, the resulting Tafel plots exhibited two slopes: 40 mV dec^{-1} at low overpotentials and H_{ad} coverage, and 120 mV dec^{-1} at high overpotentials and H_{ad} coverage; thus, it is probable that this is the dominant mechanism for HER on the G-PtNi/Au deposits.

As can be seen in Table 4, the material with the best catalytic properties in this work has a η_{10} value comparable to the hcp Pt–Ni nano-multipods reported by Cao et al.,[42] however, it is 25 mV higher than the lowest values reported by Xie et al.[21] and Zhao et al.[24]

The mass current density, j_m, at an overpotential of 38 mV was also used as an efficiency criterion. To obtain this value, the current was normalized to the Pt mass of the galvanostatically generated deposits, which was estimated using Faraday's law [Eq. (13)]:

$$g_{Pt} = \frac{i_{dep}\tau_{Pt}m}{nF} \tag{13}$$

where g_{Pt} is the Pt mass in grams, i_{dep} is the applied deposition current, τ_{Pt} is the Pt deposition time (taken from Table 2), and m is the atomic mass of Pt. For comparison's sake, an extreme scenario was considered in which Pt deposition proceeded at 100% efficiency during the two seconds the chronopotentiometry experiment lasted. The j_m at a 38 mV overpotential of this case is labeled "Pt max" in Table 3. Under this efficiency criterion, the catalytic activity of the PtNi deposited at 8.0 mA cm^{-2} is far superior to the material that exhibits lower η_{10} values. Even in this extreme scenario, the activity of the G-

Table 3. Tafel slopes of G-PtNi/Au generated at different j_{dep} values.

Head 1[a]	First Tafel Slope/[mv dec^{-1}]	Second Tafel Slope/[mv dec^{-1}]
2.0×10^{-3}	35.0 ± 1.4	98.8 ± 1.1
4.0×10^{-3}	34.3 ± 0.3	68.5 ± 0.7
6.0×10^{-3}	34.7 ± 0.2	95.4 ± 1.0
8.0×10^{-3}	35.1 ± 0.4	97.9 ± 1.1
10.0×10^{-3}	38.9 ± 0.3	100.6 ± 1.2

Table 4. Comparison of the galvanostatically deposited G-PtNi/Au with other PtNi material with high HER activity.

Material	η_{10}/[mV]	j_m @ η = 38 [mV/A g_{Pt}^{-1}]	Tafel slope [mVdec^{-1}]	Ref.
G-PtNi/Au 8.0 mA cm^{-2}	63	3485 51 (Pt max)	35.1 ± 0.4	This work
PtNi–Ni Na/CC[c]	38	144	57.0	[21]
Pt/C[c]	51	34.4	42.0	
PtNi NDs[b]	45	6.48	52.0	[23]
hcp Pt–Ni nano-multipods[c]	65	1080	74.0	[42]
PtNi NWs/C[a]	50	320	N.A.	[10]
Pt@2D–Ni(OH)$_2$[c]	186	858	72.0	[43]
PtNi–O[a]	38.9	1740	78.8	[24]
$Pt_{3.21}Ni@Ti_3C_2$[c]	55.6 5 mA cm^{-2}	NA	39.5	[44]

Electrolyte concentration: KOH [a] 1 M [b] 0.5 M [c] 0.1 M

PtNi/Au is higher than that for Pt/C.[21] A comparison of the Tafel slopes also positions the G-PtNi/Au as the material with high catalytic activity. This shows that galvanostatic electrodeposition can be used to synthesize PtNi materials with high catalytic activity towards HER and low Pt loading. Additionally, the synthesis is simpler than the ones used in other works; it only comprises two steps (electrochemical cleaning of the substrate and electrodeposition) and can be finished in a fraction of the time required for other methods.

The high catalytic activity of the G-PtNi/Au deposits can first be attributed to the presence of Ni and Pt on their surface, which allows a tandem operation in which Ni cleaves the HO–H bond and the recombination step occurs on the Pt surface. The thickness deposits may also be playing an important role in their performance. Kibler[45] showed that the number of Pd layers on Pd/Au(111) catalyst had an important impact on its catalytic activity for HER in acidic media.

It is important to stress the importance of galvanostatic control as the electrodeposition technique since it allows the working electrode to follow complex potential transients, resulting in materials that would be difficult to replicate by conventional potential control techniques.

Conclusion

Galvanostatic electrodeposition was used to synthesize thin PtNi films onto gold electrodes. Thanks to this method, it was possible to obtain materials with a small Tafel slope, large j_m, binder free, and with a synthesis time considerably shorter than other methods reported in the literature. The addition of small quantities of Ni was enough to significantly increase the activity of Pt. The magnitude of the deposition current density had a strong effect on η_{10} value, with the best catalyst being the one synthesized at 8.0 mA cm^{-2}. Tafel analysis suggests that HER on these materials follows a Volmer–Heyrovsky mechanism, regardless of the deposition current density.

Experimental Section

All glassware was cleaned by soaking it in 1 M KOH for 24 h and rinsing it with deionized water from an EASYpure II purification system (18.2 MΩ cm). All the electrolytes were prepared with deionized water; H_2SO_4 (Fermont, ppb trace impurities), $NiCl_2$ (CTR Scientific), $K_2[PtCl_4]$ (Sigma-Aldrich 98%), NaCl (CTR Scientific 99.9%), KOH (Sigma-Aldrich 90%) were used without additional purification. The electrolytes were saturated with N_2 before their use.

The working electrode was a gold disk with a 0.5 mm diameter fabricated by embedding a gold wire in epoxy resin, leaving a circular cross-section exposed with a geometrical area of 2.0×10^{-3} cm^2. All the experiments were performed using a three-electrode single-compartment arrangement with a Pt coil as a counter electrode. The electrochemical cleaning and electrodeposition steps were done in a cylindrical glass cell; a cylindrical Teflon cell was used for the HER measurements and all experiments in which the electrolyte was 1 M KOH. The electrochemical cleaning and electrodeposition stages were performed with a $Hg|Hg_2SO_4$ sat. K_2SO_4 reference electrode (MMSE) [0.640 V vs. NHE] and the HER stage with a Ag|AgCl sat. KCl [0.222 V vs. NHE] reference electrode. The disk electrode was polished with alumina slurries of progressively smaller particle sizes (1, 0.3, and 0.1 μm) until a mirror finish was achieved. Subsequently, it was sonicated in acetone, isopropanol, methanol, and deionized water. The electrodes were then electrochemically cleaned in 50 mM H_2SO_4 (Fermont, ppb trace impurities) by repetitive cycling between −0.70 V and 1.06 V versus MMSE (−0.06 V and 1.70 V vs. RHE) at 0.10 V s^{-1} until a stable voltammogram was obtained. Finally, a single cycle was run at 0.05 V s^{-1} to compute the working electrode's electroactive surface area (ECSA). In this case, the charge under the cathodic peak is divided by Q_0 (equation 11), which is the charge associated with the reduction of a gold oxide monolayer per square centimeter (390×10^{-6} C cm^{-2}).[27] The average surface area after 30 measurements was $6.7\pm1.8\times10^{-3}$ cm^2, which translates into a roughness factor between 3 and 4.

Electrodeposition of PtNi. After electrochemically cleaning the working electrode, the electrolyte was replaced for the platting bath, a solution containing 50 mM $NiCl_2$ + 1.5 mM $K_2[PtCl_4]$ + 500 mM NaCl, the *p*H 2.0 (adjusted with a 0.5 M H_2SO_4 solution), and bubbled with N_2 for 10 minutes. A galvanostatic pulse was applied through the working electrode; first, the electrode is held at the open-circuit voltage for 10 seconds as a stabilizing step, followed by a two-second deposition pulse. The magnitude of the latter was varied to study its effect on the electrocatalytic activity of the deposit. Since the current is an extensive property, the applied current density, j_{dep}, was chosen as the control variable. The experimentally applied current was computed by multiplying the selected j_{dep} value by the *ECSA* previously determined.

Electrocatalytic Activity for HER. The electrocatalytic performance of the as-prepared deposits was tested in a 1 M KOH solution. The electrode was first cycled 30 times at 0.05 V s^{-1} from 0 to −1.10 V versus Ag|AgCl as a conditioning step. Then, a 0.005 V s^{-1} potential scan from −0.40 to −1.10 V versus Ag|AgCl was performed.

The presence of Ni in the deposit was confirmed by cyclic voltammetry by the oxidation and reduction processes observed between −0.60 and 0.55 V versus Ag|AgCl at 0.05 V s^{-1}, in 1 M KOH. Following this, the electrode was cycled in 50 mM H_2SO_4, between −0.70 V to 1.06 V versus MMSE at 0.05 V s^{-1}, to confirm Pt deposition through the adsorption of hydrogen on its surface.

A PtNi deposit was generated by applying an 8.0 mA cm^{-2} pulse for two seconds. This deposit was examined by scanning electron microscopy (SEM) (Nova NanoSEM 200, FEI, Japan) equipped with EDX analysis (INCA X-Sight, OXFORD instruments, England) to confirm the formation of the PtNi deposit.

Acknowledgments

The authors express their gratitude to the School of Engineering and Sciences of Tecnologico de Monterrey for the postdoctoral fellowship granted to D.A.C-Y. and for the financial support received for the development of this research through the Research Chair of Photonics and Quantum Systems.

Conflict of Interest

The authors declare no conflict of interest.

Data Availability Statement

The data that support the findings of this study are available from the corresponding author upon reasonable request.

Keywords: alkaline hydrogen evolution reaction · electrocatalysis · galvanostatic electrodeposition · platinum-nickel · water electrolysis

[1] M. S. Dresselhaus, I. L. Thomas, *Nature* **2001**, *414*, 332–337.
[2] J. A. Tuner, *Science* **1999**, *285*, 687–689.
[3] I. Staffell, D. Scamman, A. Velazquez Abad, P. Balcombe, P. E. Dodds, P. Ekins, N. Shahd, K. R. Warda *Energy Environ. Sci.* **2019**, *12*, 463–491.
[4] S. Shiva Kumar, V. Himabindu, *Mater. Sci. Energy Technol.* **2019**, *2*, 442–454.
[5] M. Schalenbach, A. R. Zeradjanin, O. Kasian, S. Cherevko, K. J. J. Mayrhofer, *Int. J. Electrochem. Sci.* **2018**, *13*, 1137–1226.
[6] P. A. Thiel, T. E. Madey, *Surf. Sci. Rep.* **1987**, *7*, 211–385.
[7] M. A. Henderson, *Surf. Sci. Rep.* **2002**, *46*, 1–308.
[8] J. B. Raoof, R. Ojani, S. A. Esfeden, S. R. Nadimi, *Int. J. Hydrogen Energy* **2010**, *35*, 3937–3944.
[9] O. Savadogo, E. Ndzebet, *Int. J. Hydrogen Energy* **2001**, *26*, 213–218.
[10] P. Wang, K. Jiang, G. Wang, J. Yao, X. Huang, *Angew. Chem.* **2016**, 128, 1–6; *Angew. Chem. Int. Ed.* **2016**, *55*, 1–1.
[11] Y. Hao, X. Wang, Y. Zheng, J. Shen, J. Yuan, A.-j. Wang, L. Niu, S. Huang, *Int. J. Hydrogen Energy* **2016**, *41*, 9303–9311.
[12] S. Gao, X. Yang, S. Liang, Y.-H. Wang, H.-Y. Zanga, Y.-G. Lia, *Inorg. Chem. Commun.* **2019**, *106*, 104–110.
[13] Y. Zhang, F. Gao, P. Song, J. Wang, T. Song, C. Wang, C. Chen, L. Jin, L. Li, X. Zhu, Y. Du, *J. Power Sources* **2019**, *425*, 179–185.
[14] J. Chen, J. Wang, J. Chen, L. Wang, *J. Mater. Sci.* **2017**, *52*, 13064–13077.
[15] G.-R. Zhang, S. Wöllner, *Appl. Catal.* **2018**, *222*, 26–34.
[16] T. Shen, M. Chen, C. Dub, Y. Sun, Q. Tan, L. Du, G. Chen, G. Yin, *J. Alloys Compd.* **2015**, *645*, 309–316.
[17] C. Zhang, R. Zhang, X. Li, W. Chen, *ACS Appl. Mater. Interfaces* **2017**, 9, 29623–29632.
[18] H. Guan, Y. Zhao, J. Zhang, Y. Liu, S. Yuan, B. Zhang, *Sens. Actuators B* **2018**, *261*, 354–363.
[19] Y. Sun, M. Luo, Y. Qin, S. Zhu, Y. Li, N. Xu, X. Meng, Q. Ren, L. Wang, S. Guo, *ACS Appl. Mater. Interfaces* **2017**, 9, 34715–34721.
[20] X. Yu, J. Zhao, L.-R. Zheng, Y. Tong, M. Zhang, G. Xu, C. Li, J. Ma, G. Shi, *ACS Energy Lett.* **2018**, *3*, 237–244.
[21] L. Xie, Q. Liu, X. Shi, A. M. Asiri, Y. Luoa, X. Sun, *Inorg. Chem. Front.* **2018**, *5*, 1365–1369.
[22] J. Li, L. Liu, Y. Ai, Z. Hu, L. Xie, H. Bao, J. Wu, H. Tian, R. Guo, S. Ren, W. Xu, H. Sun, G. Zhang, Q. Liang, *Chem. Eur. J.* **2019**, *25*, 7191–7200.
[23] X.-Y. Huang, A.-J Wang, L. Zhang, K.-M. Fang, L.-J. Wu, J.-J. Feng, *J. Colloid Interface Sci.* **2018**, *531*, 578–584.
[24] Z. Zhao, H. Liu, W. Gao, W. Xue, Z. Liu, J. Huang, X. Pan, Y. Huang, *J. Am. Chem. Soc.* **2018**, *140*, 9046–9050.
[25] M. P. Salinas-Quezada, D. A. Crespo-Yapur, A. Cano-Marquez, M. Videa, *Fuel Cells* **2019**, *19*, 587–593.
[26] S. Lucatero, G. Tamayo, D. Crespo, E. Mariño, M. Videa, *J. Mat. Electrochem. Systems* **2013**, *16*, 177–182.
[27] M. Łukaszewski, M. Soszko, A. Czerwiński, *Int. J. Electrochem. Sci.* **2006**, *11*, 4442–4469.
[28] A. J. Bard, L. R. Faulkner, in *Electrochemical Methods: Fundamentals and Applications* (Eds.: D. Harris, E. Swain, E. Aiello), Wiley, New York, **1980**, p. 639.
[29] G. T. Martínez, G. Zavala, M. Videa, *J. Mex. Chem. Soc.* **2009**, *53*, 7–11.
[30] V. A. Isaev, O. V. Grishenkova, *J. Solid State Electrochem.* **2013**, *17*, 1505–1508.
[31] J. Vanpaemel, M. H. van der Veen, S. D. Gendt, P. M. Vereecken, *Electrochim. Acta* **2013**, *109*, 411–418.
[32] J. Vanpaemel, M. Sugiura, D. Cuypers, M. H. van der Veen, S. De Gendt, P. M. Vereecken, *Langmuir* **2014**, *30*, 2047–2053.
[33] J. Lin-Cai, D. Pletcher, *J. Electroanal. Chem.* **1983**, *149*, 237–247.
[34] Y. Liu, D. Gokcen, U. Bertocci, T. W. Moffat, *Science* **2012**, *338*, 1327–1330.
[35] F. A. Möller, A. Lachenwitzer, O. M. Magnussen, R. J. Behm, *Phys. Rev. B* **1997**, *56*, 12506–12518.
[36] A. Lachenwitzer, O. M. Magnussen, *J. Phys. Chem. B* **2000**, *104*, 7424–7430.
[37] R. Oriňáková, M. Strečková, L. Trnková, R. Rozik, M. Gálová, *J. Electroanal. Chem.* **2006**, *594*, 152–159.
[38] M. A. Rahim, R. A. Hameed, M. Khalil, *J. Power Sources* **2004**, *134*, 160–169.
[39] D. Chen, S. D. Minteer, *J. Power Sources* **2015**, *284*, 27–37.
[40] R. Wang, U. Bertocci, H. Tan, L. A. Bendersky, T. P. Moffat, *J. Phys. Chem. C* **2016**, *120*, 16228–16237.
[41] T. Shinagawa, A. T. Garcia-Esparza, K. Takanabe, *Sci. Rep.* **2015**, *5*, 13801.
[42] Z. Cao, Q. Chen, J. Zhang, H. Li, Y. Jiang, S. Shen, G. Fu, B.-A. Lu, Z. Xie, L. Zheng, *Nat. Commun.* **2017**, *8*, 15131.
[43] L. Wang, Y. Zhu, Z. Zeng, C. Lin, M. Giroux, L. Jiang, Y. Han, J. Greeley, C. Wang, J. Jin, *Nano Energy* **2017**, *31*, 456–461.
[44] Y. Jiang, X. Wu, Y. Yan, S. Luo, X. Li, J. Huang, H. Zhang, D. Yang, *Small* **2019**, 1805474.
[45] L. A. Kibler, *Electrochim. Acta* **2008**, *53*, 6824–6828.

Manuscript received: October 22, 2021
Revised manuscript received: January 16, 2022